Appl Biochem Biotechnol (2012) 166:764–773
DOI 10.1007/s12010-011-9465-y

A Hydrogen Peroxide Biosensor Based on Direct Electrochemistry of Hemoglobin in Palladium Nanoparticles/Graphene–Chitosan Nanocomposite Film

Aili Sun · Qinglin Sheng · Jianbin Zheng

Received: 11 June 2011 / Accepted: 15 November 2011 /
Published online: 3 December 2011

Abstract Thermally two-dimensional lattice graphene (GR) and biocompatibility chitosan (CS) act as a suitable support for the deposition of palladium nanoparticles (PdNPs). A novel hydrogen peroxide (H_2O_2) biosensor based on immobilization of hemoglobin (Hb) in thin film of CS containing GR and PdNPs was developed. The surface morphologies of a set of representative membranes were characterized by means of scanning electron microscopy and showed that the PdNPs are of a sphere shape and an average diameter of 50 nm. Under the optimal conditions, the immobilized Hb showed fast and excellent electrocatalytic activity to H_2O_2 with a small Michaelis–Menten constant of 16 μmol L^{-1}, a linear range from 2.0×10^{-6} to 1.1×10^{-3} mol L^{-1}, and a detection limit of 6.6×10^{-7} mol L^{-1}. The biosensor also exhibited other advantages, good reproducibility, and long-term stability, and PdNPs/GR–CS nanocomposites film would be a promising material in the preparation of third generation biosensor.

Keywords Direct electrochemistry · Nanocomposite · Hemoglobin · Hydrogen peroxide · Graphene

Introduction

Graphene (GR) has attracted strong scientific and technological interest since Geim and co-workers at Manchester University first isolated single-layer samples from graphite in 2004 [1]. GR is a single layer of carbon atoms with a hexagonal arrangement in a two-dimensional lattice and is considered as "the thinnest material in our universe" [2]. The unique properties of GR include fast electron transportation, high thermal conductivity,

A. Sun · Q. Sheng · J. Zheng (✉)
Institute of Analytical Science/Shaanxi Provincial Key Laboratory of Electroanalytical Chemistry, Northwest University, Xi'an, Shaanxi 710069, People's Republic of China
e-mail: zhengjb@nwu.edu.cn

A. Sun
Department of Chemistry and Chemical Engineering, Xinxiang University, Xinxiang 453000, People's Republic of China

excellent mechanical stiffness, and good biocompatibility [3], which result in promising applications in nanocomposites [4], solar cell [5], electromechanical resonators [6], and electrochemical sensors [7, 8]. Moreover, GR is known to promote the direct electron transfer for the redox reaction of redox proteins, and the redox enzymes immobilized in graphene can retain their enzymatic activity [9–11]. However, GR is hydrophobic and tends to form agglomerates or even re-graphitizes to graphite due to the Van der Waals interactions and strong π–π stacking which may limit its further biological applications [12]. Chitosan (CS) is an abundant natural biopolymer with unique structure. It has been universally used to disperse nanomaterials and immobilize enzymes owing to its good water permeability, excellent film forming ability, biocompatibility, nontoxicity, and high mechanical strength. Xu and co-workers immobilized Hb in the hybrid nanocomposite of GR–CS and succeeded in realizing direct electron transfer [13]. The work substantiated that the GR–CS nanocomposite film could provide a favorable microenvironment for biomolecule and facilitate efficient direct electron transfer of redox biomolecules.

Electrodeposition is a simple, fast, and inexpensive method for preparation of nanosized metal particles [14, 15]. Pd is a very important and rare transition metal and has strong potential in application of chemical sensors. In order to increase its catalytic properties and applications, research is still needed.

To the best of our knowledge, the use of GR with electrodeposition of PdNPs in biosensors applications has been unexplored till now. In this work, firstly the GR–CS nanocomposite film was assembled on the surface of the glassy carbon electrode (GCE). Secondly, PdNPs were electrodeposited on the GR–CS/GCE. Thirdly, hemoglobin (Hb) was immobilized in the composites to obtain hydrogen peroxide biosensor for the detection of H_2O_2. Finally, the performance of the fabricated biosensors was investigated by cyclic voltammetry and amperometry. The results demonstrated that these nanocomposites could offer a new and promising immobilized material for the biosensor design.

Experimental

Reagents

GR was purchased from Pioneer Nanotechnology Co. (Nanjing, China). Hb (Hb, MW 64500) was purchased from Sigma (St. Louis, USA,). CS (CS, MW 5–6×10^5, > 90% deacetylation) was purchased from Shanghai Yuanju Biotechnology Co., Ltd (Shanghai, China). H_2O_2 (H_2O_2, w/w: 30%) was got from Tianjin Tianli Chemistry Reagent Co. Ltd (Tianjin, China, www.tianli-tj.com). Phosphate buffer saline (PBS) 0.1 mol L^{-1} was used as the supporting electrolyte. Other reagents were of analytical reagent grade, and doubly distilled water was used in all experiments.

Apparatus

All the electrochemical experiments were carried out on a CHI660D electrochemical workstation (Shanghai CH Instrument Co. Ltd., China) using a three-electrode system, where a standard saturated calomel electrode (SCE) served as the reference electrode, a platinum wire electrode as the auxiliary electrode, and the modified electrode GCE as the working electrode. All the potentials given in this paper were referred to the SCE. All the tested solutions were purged with highly purified nitrogen for 30 min before the experiments, and a nitrogen environment was kept over the solution during the electrochemical measurements. Scanning

electron microscopic (SEM) measurements were carried out on a JSM-6380 scanning electron microscope (JEOL, Japan) at 20 kV accelerating voltage. All electrochemical experiments were conducted at room temperature (25±2 °C).

Electrode Preparation

Prior to use, bare GCE (Φ=4 mm) was firstly polished with 0.3 and 0.05 μm alumina slurry to obtain a mirror-like surface and ultrasonically cleaned in ethanol and water thoroughly. Then it was allowed to dry at room temperature. GR was dispersed in 0.5% CS acetic acid solution with 30 min of ultrasonication to achieve 1.0 mg mL^{-1}, and 5 μL of this black suspension was cast onto the electrode by using a syringe to prepare GR–CS/GCE and dried slowly in air.

Subsequently, PdNPs were electrodeposited on the GR–CS/GCE in the mixture solution containing $PdCl_2$, H_2SO_4, and NH_4PF_6 according to Safavi et al. [16]. To get rid of deoxygenation, high pure nitrogen was bubbled thoroughly before the deposition process for at least 20 min. After electrodepositing PdNPs, the modified electrode was gently washed by deionized water and dried in air at room temperature. The electrode was denoted as PdNPs/GR–CS/GCE. Following that, Hb was dissolved in a 0.1% chitosan solution, and the Hb concentration was 6 mg mL^{-1}; 5 μL of the resulting solution was cast onto the PdNPs/GR–CS/GCE surface using a syringe, and the modified electrode was moved into a refrigerator and kept at 4 °C to dry overnight. The fabricated modified electrode was stored at 4 °C in a refrigerator when not in use. For comparison with Hb/PdNPs/GR–CS/GCE, Hb/GR–CS/GCE was prepared with the same procedures as described previously. The preparation process of modified Hb/PdNPs/GR–CS/GCE is shown in Scheme 1.

Results and Discussion

Characterization of Chitosan-Dispersed Graphene

SEM was used to characterize the surface morphologies of modified electrode. From Fig. 1a, the dispersed CS–GR film showed a clear flake-like shape and a layer structure.

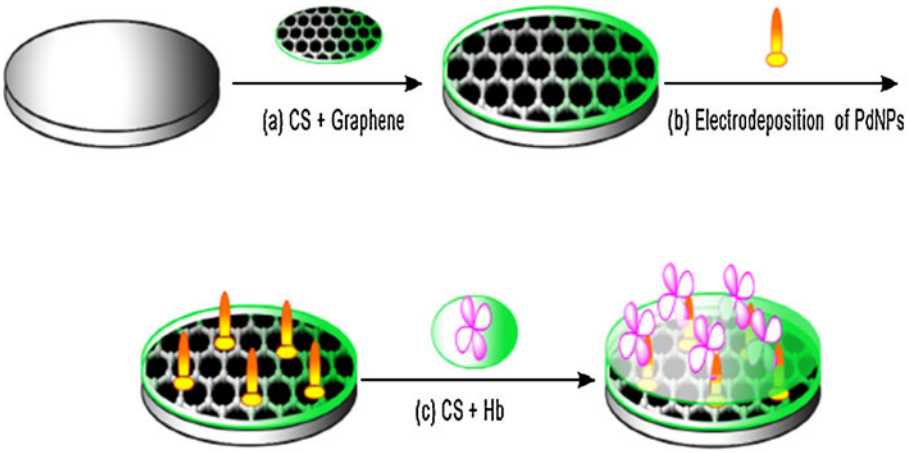

Scheme 1 The illustration of the preparation process of modified electrode

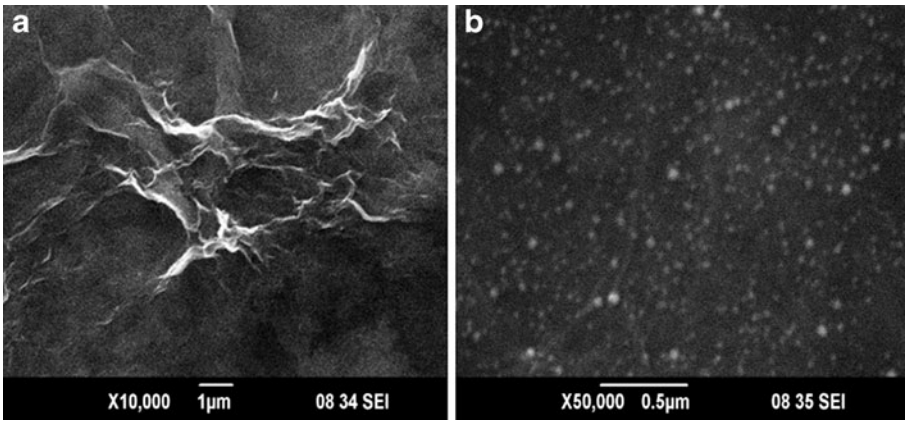

Fig. 1 SEM micrographs of **a** GR and **b** GR–PdNPs

Many spherical nanoparticles were observed with the average diameter of 50 nm (Fig. 1b), indicating that PdNPs were successfully deposited on the surface of modified electrode with a homogeneous diameter and well distribution.

EIS Characterization of Stepwise Self-Assembly Procedure

Electrochemical impedance spectroscopy (EIS) is regarded as an effective method to characterize the interface properties of surface-modified electrodes. As shown in Fig. 2, the impedance spectra include a semicircle portion and a linear portion; the semicircle part at the higher frequencies corresponds to the electron-transfer-limiting electrochemical process, and the linear part at the lower frequencies corresponds to the diffusion-limiting electrochemical process. The semicircle diameter equals the interfacial electron transfer resistance (R_{et}).

It could be seen that the bare GCE exhibited an almost straight line, which is characteristic of a diffusional limiting step of the electrochemical process. After dripping

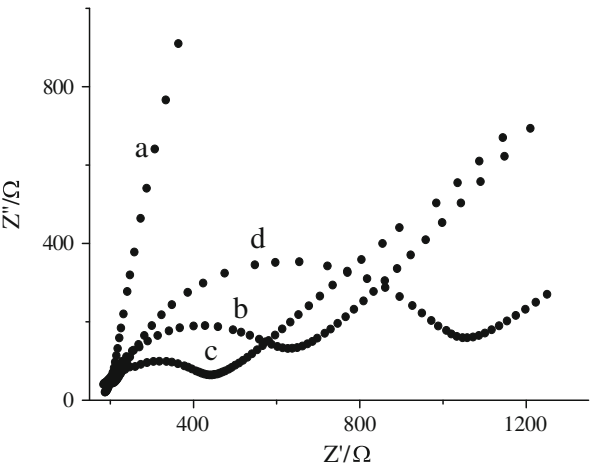

Fig. 2 EISs of bare GCE (*a*), GR–CS/GCE (*b*), PdNPs/GR–CS/GCE (*c*), and Hb/PdNPs/GR–CS/GCE (*d*) in a solution of 1.0 mmol L^{-1} $[Fe(CN)_6]^{3-/4-}$+0.1 mol L^{-1} KCl as the supporting electrolyte

GR–CS nanocomposite film on the surface of the electrode, an obvious interfacial R_{et} was observed (Fig. 2b), which was due to that GR–CS nanocomposite film formed an insulating layer on the electrode surface and obstructed the electron-conductor of the redox probe. However, when PdNPs were electrodeposited on the GR–CS/GCE, the R_{et} was decreased obviously (Fig. 2c), which proved that the PdNPs film was beneficial to the electron transfer. After the Hb and CS were dropped on the electrode surface, an obvious increase of R_{et} (Fig. 2d) was observed, which suggested that Hb and CS were successfully assembled on the surface of the resulting electrode. These results could clearly confirm that the modified electrode was successfully fabricated.

Electrochemical Characteristics of the Modified Electrode

Figure 3 shows the cyclic voltammograms (CVs) of the different electrodes in 0.1 M PBS (pH 7.0). As can be seen, no redox peak is observed at bare GCE (curve *a*). The Hb/GR–CS/GCE (curve *b*) displayed a pair of small redox peaks, which indicated that the direct electron transfer of Hb with GR–CS/GCE was achieved with a slow electron transfer rate. Whereas, under the same condition, Hb/PdNPs/GR–CS/GCE presented a pair of well-defined and quasi-reversible redox peaks corresponding to Hb Fe(III)/Fe(II) redox couples (curve *c*). The formal potential ($E^{0\prime}$) of Hb/PdNPs/GR–CS/GCE calculated by averaging the cathodic and anodic peak potentials was estimated as −0.24 V (vs. SCE). The peak-to-peak separation was about 0.162 V. The results revealed that PdNPs/GS–CS nanocomposite could greatly promote the direct electron transfer between Hb and electrode.

Effect of Scan Rate

Figure 4 shows the CVs of the Hb/PdNPs/GR–CS/GCE recorded in 0.1 mol L^{-1} PBS (pH 7.0). It was found that both anodic and cathodic peak currents increased clearly with the increase of the scan rate. The peak currents were linearly correlated to the square root of the scan rate in the range from 0.1 to 1.5 $V s^{-1}$ (insert of Fig. 4). The linear regression equation was I_{pa} (μA)=−6.477−2.15v (V s^{-1}) (n=15, r=0.9935) and I_{pc} (μA)=10.65+2.72v (V s^{-1})

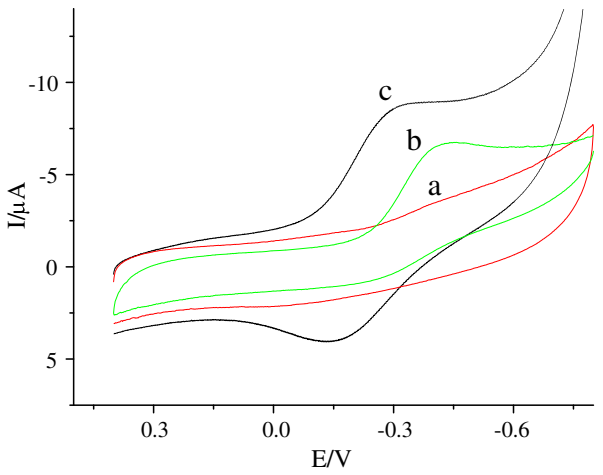

Fig. 3 CVs of bare GCE (*a*), Hb/GR–CS/GCE (*b*), and Hb/PdNPs/GR–CS/GCE (*c*) in pH 7.0 PBS at a scan rate of 0.50 $V s^{-1}$

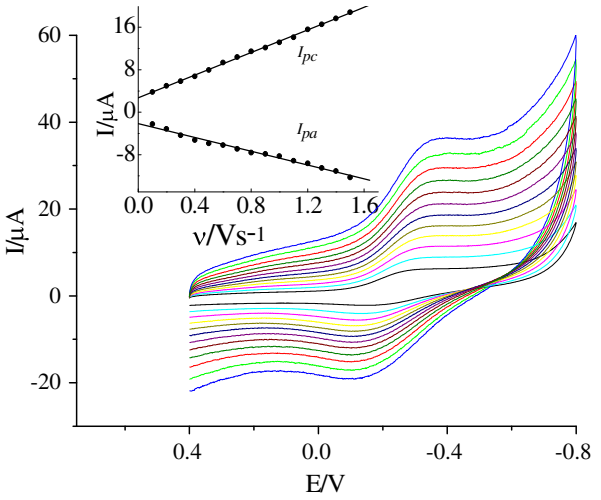

Fig. 4 CVs of Hb/PdNPs/GS–CS/GCE in pH 7.0 PBS with different scan rates (from *a* to *o*): 0.1, 0.2, 0.3, 0.4, 0.5, 0.6, 0.7, 0.8, 0.9, 1.0, 1.1, 1.2, 1.3, 1.4, and 1.5 Vs^{-1}

(n=15, r=0.9993), implying that the electrochemical kinetics was a diffusion-controlled process. According to the Laviron's equation [17]:

$$I_p = n^2F^2A\Gamma v/4RT. \tag{1}$$

From the slope of the I_{pc}–v curve, n was calculated to be 0.88, meaning that one electron transfer was involved. The surface concentration of electroactive Γ^* was calculated from the following equation [18]:

$$\Gamma^* = Q/nFA \tag{2}$$

where Q is the charge involved in the reaction, A is the geometric area of the GCE, n is the number of the electron transferred, F is the Faraday constant, and Γ^* is the surface concentration of the electroactive substance. The surface coverage of electroactive Hb Γ^* at Hb/PdNPs/GR–CS/GCE was calculated to be 1.74×10^{-10} mol cm^{-2}, which was much larger than that of monolayer coverage (1.89×10^{-11} mol cm^{-2} for Hb) [19].

The electron transfer rate constant (k_s) of Hb on the modified electrode could be obtained by the following equation [20]:

$$E_{pc} = E^{0'} - \frac{RT}{\alpha nF}\log v \tag{3}$$

$$E_{pa} = E^{0'} + \frac{RT}{(1-\alpha)nF}\log v \tag{4}$$

$$\log k_s = \alpha\log(1-\alpha) + (1-\alpha)\log\alpha - \log(RT/nFv) - (1-\alpha)\alpha F\Delta E_p/(2.3RT) \tag{5}$$

where α is the charge transfer coefficient, and n is the number of electron transfer. R, T, and F have their conventional meanings. ΔE_p is the peak-to-peak potential separation. With the increase of the scan rate, the redox peak potentials were also shifted gradually. The relationships of E_{pa} and E_{pc} with log$v$ were constructed with the linear regression equations

E_{pa} (V)=0.1715 log$v$−0.0479 (n=16, r=0.9935) and E_{pc} (V)=−0.3628 log$v$−0.0645 (n=16, r=0.9993). According to Eqs. 3, 4, and 5, α was calculated as 0.42, and the electron transfer rate constant (k_s) was further estimated to be 0.86 s^{-1}, which was much larger than that of Hb immobilized in carbon nanotube powder microelectrodes electrodes of 0.062 s^{-1} [21] and Hb immobilized in AuNPs of 0.49 s^{-1} [22]. At the same time, the value of electron transfer rate constants of Hb/GR–CS/GCE was estimated to be 0.69 s^{-1}, which was smaller than immobilization of Hb in PdNPs/GR–CS nanocomposite film. Thus, GR and PdNPs could provide a microenvironment for Hb to undergo a facile electron transfer reaction.

Influence of pH Value

The dependence of the biosensor response on pH value of the measurement solution was investigated. The pH value of the solution ranged from 4.5 to 9.0. The current response increased from pH 4.5 and reached the maximum at pH 7.0. Then, the current response decreased from pH 7.0 to 9.0. The reason might be that a strong acidic or alkaline solution would decrease the bioactivity of Hb, leading to an obvious decrease in the response current. Therefore, the suitable pH 7.0 of the working buffer was selected.

Amperometric Response of the Hb/PdNPs/GR–CS/GCE Toward H_2O_2

Figure 5 shows a typical current–time curve of the biosensor under the optimized experimental conditions after the addition of successive H_2O_2 concentration to the PBS under stirring. With the increase of the concentration of substrate, the response current of the biosensor reached 95% of the steady state value within 6 s, indicating that a rapid response occurred. The inset of Fig. 5 displays the calibration curve of the biosensor for H_2O_2 determination. The response current increased linearly with the H_2O_2 concentration in the range from 2.0×10^{-6} to 1.1×10^{-3} mol L^{-1}, with a correlation coefficient of 0.9984, and the detection limit of 6.6×10^{-7} mol L^{-1} is estimated at a signal-to-noise ratio of 3. From the slope of 5.40×10^{-3} 16 μA μM^{-1}, the sensitivity of the proposed Hb biosensor was 0.20 A M^{-1} cm^{-2}, which was larger than 0.06 A M^{-1} cm^{-2}.

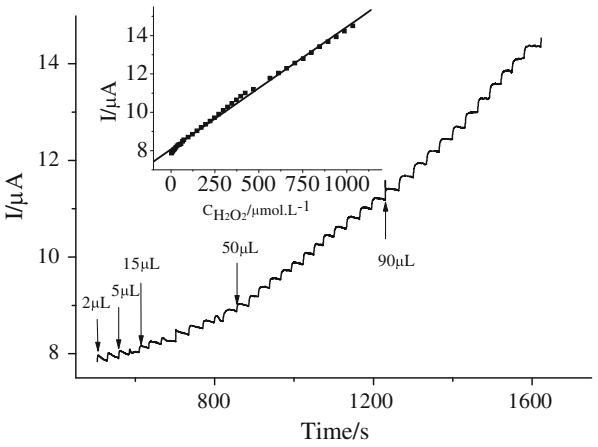

Fig. 5 Amperometric response of Hb at the Hb/PdNPs/GS–CS/GCE when successively adding different amounts of H_2O_2 into 25 mL stirring PBS (pH 7.0) at the potential of −0.35 V. *Inset*: the corresponding calibration curve

When the concentration of H_2O_2 was more than 1.1×10^{-3} mol L^{-1}, a response plateau was observed, showing a typical Michaelis–Menten kinetic mechanism. The apparent Michaelis–Menten constant (K_M^{app}) could be calculated by the Lineweaver–Burk equation [23]:

$$1/I_{ss} = 1/I_{max} + K_M{}^{app}/(I_{max}C) \quad (6)$$

Here I_{ss} is the steady-state current after the addition of the substrate, C is the bulk concentration of the substrate, and I_{max} is the maximum current measured under the saturate substrate conditions. The value of K_M^{app} and I_{max} could be obtained by the slope and the intercept of the plot of the reciprocals of the steady-state current versus H_2O_2 concentration. According to this method, the K_M^{app} value was calculated as 16 μmol L^{-1}, which was much lower than that in some previous reports [24, 25]. Since the smaller K_M^{app} represents higher catalytic ability, we can conclude that the PdNPs/GR–CS nanocomposite film would display a higher affinity and enzymatic activity.

The possible mechanism of electrocatalytic reduction of H_2O_2 at Hb-based electrode has been reported [26]:

$$\mathrm{Hb[Heme(FeIII)] + H_2O_2 \rightarrow Compound\,I + H_2O} \quad (7)$$

$$\mathrm{Compound\,I + H_2O_2 \rightarrow Hb[Heme(FeIII)] + H_2O + O_2} \quad (8)$$

$$\mathrm{Hb[Heme(FeIII)] + H+ + e- \rightarrow Hb[Heme(FeII)]\ at\ electrode} \quad (9)$$

$$\mathrm{Hb[Heme(FeII)] + O_2 \rightarrow Hb[Heme(FeII)] - O_2\ \ fast} \quad (10)$$

$$\mathrm{Hb[Heme(FeII)] - O_2 + H+ + e- \rightarrow Hb[Heme(FeIII)] + H_2O_2\ at\ electrode} \quad (11)$$

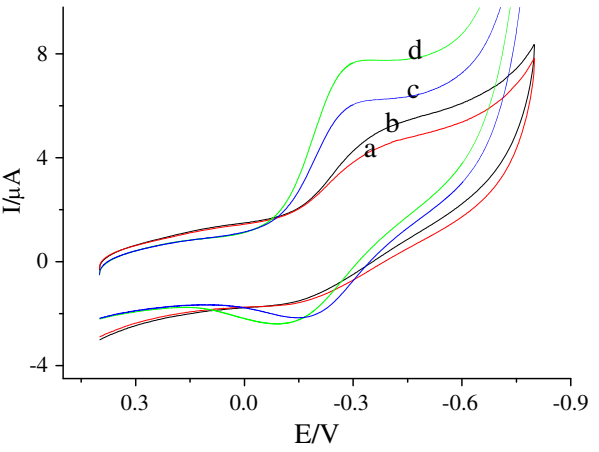

Fig. 6 CVs of Hb/GS–CS/GCE (*a*) and Hb/PdNPs/GS–CS/GCE (*c*) without H_2O_2 and in the presence of 40 μM H_2O_2 Hb/GS–CS/GCE (*b*) and Hb/PdNPs/GS–CS/GCE (*d*). Scan rate: 0.10 Vs^{-1}

The overall reaction of Eqs. 7, 8, 9, 10, and 11 would be:

$$H_2O_2 + 2H + +2e- \rightarrow 2H_2O \quad (12)$$

For comparison, the electrocatalytic activity of the Hb/PdNPs/GS–CS/GCE and Hb/GS–CS/GCE toward the same concentrations of H_2O_2 was also investigated (Fig. 6). It was found that the electrode modified with GS–CS nanocomposite film showed a relatively small current response to H_2O_2 than PdNPs/GS–CS nanocomposite film. The results revealed that the PdNPs/GS–CS nanocomposite film exhibited a better catalytic property due to the synergistic effect of the PdNPs and GS–CS nanocomposite film.

Repeatability and Stability of the Hydrogen Peroxide Biosensor

The concentration of 0.10 mmol L^{-1} H_2O_2 was measured consecutively for ten times, and a relative standard deviation (RSD) of 4.2% was obtained, indicating that the biosensor showed a good reproducibility for the determination of H_2O_2 in its linear range.

Stability was a basic requirement for fabrication of H_2O_2 biosensors. The stability of the proposed biosensor was examined through the response to 0.10 mmol L^{-1} H_2O_2. The results revealed that the current response only decreased 7.5% of its initial value after a storage period of 15 days and 14% after a storage period of 1 month, indicating that the biosensor had good stability.

Real Sample Analysis and Selectivity Against Interferences

The real analytical applicability of the proposed biosensor was examined by the determination of H_2O_2 level in reagent H_2O_2. The results obtained by the biosensor were compared with those determined by the classical $KMnO_4$ titration method. The results were in acceptable agreement, and the modified electrode could be used for the H_2O_2 sample analysis.

To evaluate the selectivity of the biosensor, the influence of some possible interfering substances, such as ascorbic acid, glucose, uric acid, L-cysteine and L-tyrosine were examined. When 0.2 mmol L^{-1} of interfering substance was added to the PBS containing 1.0 mmol L^{-1} H_2O_2, respectively, it caused a decrease of 1.9%, 2.7%, 3.1 %, 3.5%, and 3.3% in the reduction current of 1.0 mM H_2O_2, indicating that the proposed biosensor had high selectivity.

Conclusions

A novel hydrogen peroxide biosensor was constructed based on Hb which was successfully immobilized at GCE modified with new PdNPs/GR–CS nanocomposite film, and the direct electron transfer between Hb and the GCE was realized. This biosensor showed highly catalytic activity to H_2O_2 with a wider linear range, lower detection limit, and smaller K_M^{app} value of 16 μmol L^{-1}. This was attributed to that the PdNPs/GR–CS nanocomposite not only could offer a favorable environment to immobilized Hb but also facilitated the electron transfer between Hb and underlying GCE. The hybrid material could provide a good electrochemical sensing platform for the applications in biosensor and biocatalysis.

Acknowledgements The authors appreciate the financial support from the National Natural Science Foundation of China (No. 20875076) and the Scientific Initializing Foundation of Northwest University (No. PR09036).

References

1. Novoselov, K. S., KGeim, A., Morozov, S. V., Jiang, D., Zhang, Y., Dubonos, S. V., Grigorieva, I. V., & Firsov, A. A. (2004). *Science, 306*, 666–669.
2. Geim, A. K., & MacDonald, A. H. (2007). *Physics Today, 60*, 35–41.
3. Chen, H., Müller, M. B., Gilmore, K. J., Wallace, G. G., & Li, D. (2008). *Advanced Materials, 20*, 35–57.
4. Stankovich, S., Dikin, D. A., Dommett, G. H. B., Kohlhaas, K. M., Zimney, E. J., Stach, E. A., Piner, R. D., Nguyen, S. T., & Ruoff, R. S. (2006). *Nature, 442*, 282–286.
5. Wu, J. B., Becerril, H. A., Bao, Z. A., Liu, Z. F., Chen, Y. S., & Peter, P. (2008). *Applied Physics Letters, 92*, 263–302.
6. Bunch, J. S., Vander, Z. A. M., Verbridge, S. S., Frank, I. W., Tanenbaum, D. M., Parpia, J. M., Craighead, H. G., & McEuenh, P. L. (2007). *Science, 315*, 490–493.
7. Chen, L. Y., Tang, Y. H., Wang, K., Liu, C. B., & Luo, S. L. (2011). *Electrochemistry Communications, 13*, 133–137.
8. Ahmad, M., Pan, C. F., Gan, L., Nawaz, Z., & Zhu, J. (2010). *Journal of Physical Chemistry C, 114*, 243–250.
9. Shan, C., Yang, H., Song, J., Han, D., Ivaska, A., & Niu, L. (2009). *Analytical Chemistry, 81*, 2378–2382.
10. Zuo, X., He, S., Li, D., Peng, C., Huang, Q., Song, S., & Fan, C. (2010). *Langmuir, 26*, 1936–1939.
11. Kang, X., Wang, J., Wu, H., Aksay, I., Liu, A. J., & Lin, Y. (2009). *Biosensors & Bioelectronics, 25*, 901–905.
12. Niyogi, S., Bekyarova, E., Itkis, M. E., McWilliams, J. L., Hamon, M. A., & Haddon, R. C. (2006). *Journal of American Chemical Society, 24*, 7720–7721.
13. Xu, H. F., Dai, H., & Chen, G. N. (2010). *Talanta, 81*, 334–338.
14. Cattarin, S., & Musiani, M. (2006). *Electrochimica Acta, 52*, 1339–1348.
15. Riley, D. J. (2002). *Opin. Curr. Journal of Colloid and Interface Science, 7*, 186–192.
16. Safavi, A., Maleki, N., Tajabadi, F., & Farjami, E. (2007). *Electrochemistry Communications, 9*, 1963–1968.
17. Laviron, E. (1979). *J Electroanal. Chem, 100,* 263–270.
18. Zhang, Y. H., Chen, X., & Yang, W. S. (2008). *Sensors and Actuators B, 130*, 682–688.
19. Wang, S. F., Chen, T., Zhang, Z. L., Shen, X. C., Lu, Z. X., Pang, D. W., & Wong, K. Y. (2005). *Langmuir, 21*, 9260–9266.
20. Laviron, E. (1979). *Electrochemistry Communications, 101*, 19–28.
21. Zhao, Y. D., Bi, Y. H., Zhang, W. D., & Luo, Q. M. (2005). *Talanta, 65*, 489–494.
22. Gu, H. Y., Yu, A. M., & Chen, H. Y. (2001). *Journal of Electroanalytical Chemistry, 516*, 119–126.
23. Kamin, R. A., & Willson, G. S. (1980). *Analytical Chemistry, 52*, 1R–9R.
24. Fan, C. H., Wang, H. Y., Sun, S., Zhu, D. X., Wagner, G., & Li, G. X. (2001). *Analytical Chemistry, 73*, 2850–2854.
25. Wang, Y. Y., Chen, X. Y., & Zhu, J. J. (2009). *Electrochemistry Communications, 11*, 323–326.
26. Lu, X. B., Zhang, H. J., & Ni, Y. W. (2008). *Biosensors & Bioelectronics, 24*, 93–98.